BIOCHEMISTRY
including biophysical chemistry & molecular biology

Article

pubs.acs.org/biochemistry

Structural Characterization of the C3 Domain of Cardiac Myosin Binding Protein C and Its Hypertrophic Cardiomyopathy-Related R502W Mutant

Xiaolu Linda Zhang,[†] Soumya De,[‡] Lawrence P. McIntosh,*[,‡] and Mark Paetzel*[,†]

[†]Department of Molecular Biology and Biochemistry, Simon Fraser University, South Science Building, 8888 University Drive, Burnaby, British Columbia, Canada V5A 1S6

[‡]Department of Biochemistry and Molecular Biology, Department of Chemistry, and The Michael Smith Laboratories, University of British Columbia, Vancouver, British Columbia, Canada V6T 1Z3

Supporting Information

ABSTRACT: Human cardiac myosin binding protein C (cMyBP-C), a thick filament protein found within the sarcomere of cardiac muscle, regulates muscle contraction and is essential for proper muscle function. Hypertrophic cardiomyopathy (HCM), a genetic disease affecting 1 in 500 people, is the major cause of death in young athletes. It is caused by genetic mutations within sarcomeric proteins. Forty-two percent of the HCM-related mutations are found in cMyBP-C. Here we present the nuclear magnetic resonance-derived structural ensembles of the wild-type cMyBP-C C3 domain and its HCM-related R502W mutant. The C3 domain adopts an immunoglobulin-like fold, and mutation of the exposed Arg502 to a tryptophan does not perturb its structure, dynamics, or stability. However, the R502W mutation does alter the predicted electrostatic properties of the C3 domain. We hypothesize that this mutation, and other HCM-linked mutations found within the same domain, may directly disrupt the interaction of cMyBP-C with other sarcomeric proteins.

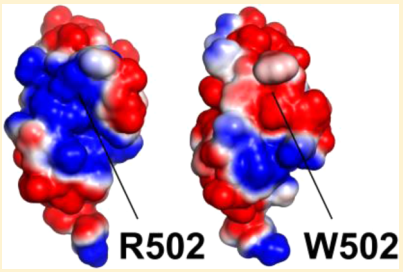

Cardiac myosin binding protein C (cMyBP-C) is essential for the regulation of contractility in cardiac muscle.[1] When cMyBP-C is knocked out in mice, the sarcomere still assembles but the animals show cardiac hypertrophy and impaired contractile function.[2] *MYBPC3*, the gene that encodes cMyBP-C, is closely linked with hypertrophic cardiomyopathy (HCM). This genetic disease is caused mostly by mutations within cardiomyocyte sarcomeric proteins, including cMyBP-C.[3] HCM is a leading cause of sudden cardiac death in young people and athletes, occurring in 0.2% of the general population.[4] Approximately 42% of the HCM-related mutations are found in the *MYBPC3* gene.[5,6] One such mutation, R502W, first reported in a patient with hypertrophic cardiomyopathy in 2003 by Richards et al.,[7] lies within the C3 domain of cMyBP-C. This mutation is caused by a C10951T nucleotide change within exon 17 of *MYBPC3*.[7] The mechanism of how this and related missense mutations affect the function of cMyBP-C and subsequently impair contractility is unclear.

cMyBP-C is located on the thick filaments of vertebrate cardiac muscle and appears as seven to nine stripes, approximately 43 nm apart, in the cross-bridging C zones of the sarcomere.[8−10] It is a 130 kDa modular protein, predicted by sequence analysis to be comprised of eight immunoglobulin-like (Ig-like) domains and three fibronectin-like domains[11] (Figure 1). cMyBP-C has an additional N-terminal domain, C0, as well as four phosphorylation sites in a mybpc motif and a 28-residue insert in the C5 domain as compared to the skeletal isoform.[12] Co-sedimentation experiments and immunofluorescence microscopy of recombinant proteins have revealed that the C-terminal portion (C7−C10) of cMyBP-C is tethered to the myosin backbone.[13−15] The N-terminal region of cMyBP-C functions in modulating contractility by interacting with the S2 region of myosin in a phosphorylation-controlled manner.[16,17] Studies have also shown that a (Pro-Ala)-rich sequence within cMyBP-C interacts with actin[17,18] and tropomyosin.[19] Thus, the C1 domain and mybpc motif may also provide a platform for actin binding.[20,21] A three-dimensional (3D) electron microscopy reconstruction confirmed that N-terminal fragments of cMyBP-C (C0−C3) lie alongside F-actin.[22]

In this study, we have determined the three-dimensional structural ensembles of the cMyBP-C C3 domain and its HCM-related R502W mutant by NMR spectroscopy. We also investigated their dynamic properties and relative thermal stabilities. In addition to confirming that the C3 domain adopts an Ig-like fold, our results show that the substitution of a positively charged arginine with a hydrophobic/aromatic tryptophan does not result in any significant perturbations of its structure, dynamics, or stability. Accordingly, we hypothesize that the R502W mutation alters the interactions of the cMyBP-C C3 domain with its binding partner proteins. This likely results, in part, from a change in the electrostatic surface of the cMyBP-C C3 domain due to the mutation. Our research

Received: June 24, 2014
Revised: July 22, 2014
Published: July 24, 2014

   dx.doi.org/10.1021/bi500784g | *Biochemistry* 2014, 53, 5332−5342

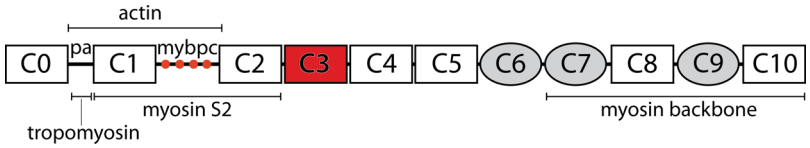

Figure 1. Schematic representation of the modular architecture of cMyBP-C. Fibronectin-like domains are shown as gray ovals and immunoglobulin-like domains as rectangles, with C3 colored red. The four phosphorylation sites within the mybpc motif are shown as red dots, and the (Pro-Ala)-rich sequence is shown as "pa". Regions of interaction on cMyBP-C, as reported in the literature, are indicated with horizontal bars and labeled with the names of the interacting proteins.

Table 1. Summary of Structural Statistics for the cMyBP-C C3 Domains

	WT (PDB entry 2MQ0)	R502W mutant (PDB entry 2MQ3)
summary of restraints		
NOE distance restraints		
intraresidue	471	356
sequential	626	384
medium-range ($1 < \|i - j\| < 5$)	294	152
long-range ($\|i - j\| \geq 5$)	1103	520
total	2494	1412
dihedral angle restraints		
φ, ψ	86, 88	83, 85
Ramachandran analyses (%)		
residues in most favored regions	92.3	92.6
residues in allowed regions	7.7	7.4
residues in generously allowed and disallowed regions	0.0	0.0
violations (average ± standard deviation)		
distance restraints (Å)	0.12 ± 0.28	0.06 ± 0.21
dihedral angle restraints (deg)	0.47 ± 1.57	0.31 ± 0.82
deviations from idealized geometry		
bond lengths (Å)	0.004	0.004
bond angles (deg)	0.6	0.6
root-mean-square deviation (Å)[a]		
backbone atoms (C, N, O)	0.61 ± 0.09	0.80 ± 0.12
all atoms (C, N, O)	0.84 ± 0.12	1.19 ± 0.12

[a]Pairwise root-mean-square deviation calculated among 10 refined structures for residues 454−538 of the human cMyBP-C C3 domain.

provides a molecular framework for understanding the role of the R502W mutation, and other related mutations, within cMyBP-C C3 domain linked to cardiomyopathy.

EXPERIMENTAL PROCEDURES

Cloning and Mutagenesis. A 273 bp DNA fragment, encoding the C3 region (residues 453−543) of human cMyBP-C, was amplified from the full-length *MYBPC3* cDNA gene. The polymerase chain reaction (PCR) used the forward primer 5′-GCCATATGCCTGTGCTCATCACGCG-3′ and the reverse primer 5′-GCGCGGCCGCTTACTTTTCCTGCACA-ATGAGCT-3′ that contain the *Nde*I and *Not*I restriction sites, respectively. The PCR product was ligated into the pET28a vector (Novagen). The resulting construct, denoted as His_6-C3, encodes the WT C3 domain of cMyBP-C with a cleavable N-terminal hexahistidine affinity tag. Subsequent DNA sequencing (GENEWIZ) confirmed that the C3 insert matched the sequence reported in the Swiss-Prot database (UniProt entry Q14896/MYBPC3_HUMAN). The R502W C3 construct was made from the WT C3 construct by site-directed mutagenesis using primers 5′-GACCTTCAAATACTGGTTCAAGAAGG-ACGG-3′ and 5′-CCGTCCTTCTTGAACCAGTATTTGAA-GGTC-3′.

Isotopic Labeling and Protein Purification. The expression plasmids were transformed into *Escherichia coli* BL21(λDE3) cells. Uniformly ^{15}N-labeled His_6-C3 was expressed in M9T medium (200 μg/mL kanamycin) supplemented with 1 g/L $^{15}NH_4Cl$ (Sigma-Aldrich). Uniformly ^{13}C- and ^{15}N-labeled His_6-C3 was expressed in M9T medium containing 3 g/L [$^{13}C_6$]glucose (Sigma-Aldrich) and 1 g/L $^{15}NH_4Cl$. For both isotopically labeled samples, cultures were grown at 37 °C to an OD_{600} of 0.6 and induced with 1 mM IPTG. After an overnight incubation, cells were harvested by centrifugation at 6000*g* (4 °C) for 7 min and subsequently lysed using an Avestin Emulsiflex-3C high-pressure homogenizer at 15000−20000 psi for 5 min in 50 mM sodium phosphate buffer (pH 6.5). The resulting lysate was further centrifuged at 29000*g* for 30 min at 4 °C. The supernatant containing the His_6-tagged proteins was loaded onto a Ni^{2+} affinity column [column volume of 5 mL (GE Healthcare)], pre-equilibrated with phosphate buffer. Elution was performed in five steps with an increasing imidazole concentration (from 100 to 500 mM, in 100 mM increments). Samples of the elution fractions were run on a 15% sodium dodecyl sulfate−polyacrylamide gel electrophoresis (SDS−PAGE) gel. Fractions containing C3 were combined and concentrated to 5 mL using an Amicon centrifugal filter unit (5 kDa cutoff, Millipore). The His_6 tag was cleaved by adding 10 units (1 unit/uL) of thrombin and incubating for 6 h. The protein was then further purified using a size-exclusion chromatography column (HiPrep 26/60 Sephacryl S-100 High-Resolution) on an ÄKTAprime system (Pharmacia Biotech). The column was equilibrated with

dx.doi.org/10.1021/bi500784g | *Biochemistry* 2014, 53, 5332−5342

50 mM sodium phosphate buffer (pH 6.5) and 100 mM NaCl and run at a flow rate of 1.0 mL/min. Fractions containing C3 were identified using 15% SDS−PAGE, pooled, and concentrated to 10 mg/mL using an Amicon ultracentrifugal filter device (3 kDa cutoff, Millipore). The final protein (Pro453−Lys543) with four remnant N-terminal residues, Gly-Ser-His-Met, resulting from cloning and thrombin cleavage) is 95 residues in length and has a calculated molecular mass of 10812 Da and a calculated isoelectric point of 5.1. The concentration was determined by UV_{280} absorption with a NanoDrop ND-100 spectrophotometer (Thermo Scientific) using predicted extinction coefficients of 8480 and 13980 M^{-1} cm^{-1} for the WT and R502W species, respectively.[23]

Acquisition of NMR Data. NMR experiments were performed on TCI cryoprobe-equipped Bruker Avance III 500 and 600 MHz NMR spectrometers at 25 °C. All samples consisted of 0.8 mM protein in 50 mM sodium phosphate buffer (pH 6.5) and 100 mM NaCl with 10% D_2O. The spectra were processed with NMRPipe[24] and analyzed using Sparky.[25]

Chemical Shift Assignments and Structure Calculation. Signals from the backbone ^1H, ^{13}C, and ^{15}N nuclei of the ^{13}C- and ^{15}N-labeled WT and R502W C3 domains were assigned using the following experiments: $^{15}N/^{13}C$ HSQC, HNCO, HN(CA)CO, HNCACB, and HN(CO)CACB.[26] Aliphatic side chain assignments were obtained from 3D (H)CC(CO)NH-TOCSY, H(CC)(CO)NH-TOCSY, and HCCH-TOCSY experiments. The aromatic side chains were assigned using the two-dimensional (Hβ)Cβ(CγCδ)Hδ and (Hβ)Cβ(CγCδCε)Hε experiments.[27] Backbone dihedral angles were predicted from $^{13}C^{\alpha}$, $^{13}C^{\beta}$, $^{13}C'$, $^1H^{\alpha}$, $^1H^N$, and ^{15}N chemical shifts with TALOS+[28] and used as restraints for structure calculations. NOE-derived distance restraints were obtained from simultaneous 3D $^1H-^{15}N/^{13}C-^1H$ NOESY-HSQC (mixing time of 110 ms)[29] and methyl-NOESY spectra.[28] The NOESY spectra were partially assigned manually, followed by automated assignment using CYANA 3.0.[30] Structure calculations were performed in seven iterative cycles. Each cycle yielded 100 structures, and the 10 lowest-energy structures were taken into the following cycle as the basis for further spectral assignments and structure calculations. The 10 lowest-energy structures generated in the final cycle were then refined with CNS using explicit solvent and molecular dynamics simulations.[31] Table 1 shows a summary of the restraints and structural statistics for both proteins. The chemical shifts and structural coordinates of the WT C3 domain ensemble have been deposited in the BioMagResData Bank (accession number 25007) and the Protein Data Bank (PDB) (entry 2MQ0), respectively. The chemical shifts and structural coordinates of the R502W C3 domain ensemble have been deposited in the BioMagResData Bank (accession number 25010) and the Protein Data Bank (entry 2MQ3), respectively.

Backbone Amide ^{15}N Relaxation. Amide ^{15}N relaxation data (T_1, T_2, and heteronuclear NOE) were collected at 25 °C on the WT and R502W C3 proteins with a 500 MHz NMR spectrometer.[32] Relaxation rate constants were determined by fitting each set of peak heights to a single-exponential decay. Errors in the rate constants were determined by Monte Carlo simulations. The heteronuclear $\{^1H\}-^{15}N$ NOE values were determined from the ratio of peak height versus a control reference spectrum, and the NOE errors were estimated from the spectral noise. The global tumbling correlation times and anisotropic model-free order parameters (S^2) were calculated from the relaxation data and structural ensembles using TENSOR2.[33]

Amide relaxation-compensated ^{15}N CPMG-HSQC spectra were collected at 600 MHz. Interleaved spectra at different CPMG field strengths (ν_{CPMG} = 50, 100, 200, 400, 600, 800, and 1000 Hz) were collected in random order with a constant time delay (T_{relax}) of 80 ms.[34] Peak volumes, determined using the autoFit.tcl script of NMRPipe, were used to calculate the effective transverse relaxation rate $R_{2,eff} = (-1/T_{relax}) \ln(V_{CPMG}/V_0)$, where V_{CPMG} and V_0 are the peak volumes with and without the CPMG pulse train, respectively.

Structural and Electrostatic Analyses. The secondary structural analysis was performed using the MICS program,[35] combined with manual inspection of the backbone hydrogen bonding patterns. The root-mean-square deviation (rmsd) values reported for protein superimpositions were calculated by pairwise ensemble comparison in PyMol.[37] The DALI[36] and FATCAT[37] servers were used to find proteins with similar folds. The surface electrostatic analyses were performed with the adaptive Boltzmann-Poisson solver plug-in[38] within PyMol[39] using dielectric constants of 2 for protein and 80 for solvent. The solvent radius was set at 1.4 Å. The per-atom charge and radius were calculated using the AMBER force field[40] within PDB2PQR.[41] Default parameters were used in PDB2PQR, except for the protonation states that were assigned at pH 6.5 to match the NMR experimental conditions.

Collection and Analysis of Circular Dichroism Data. Circular dichroism (CD) spectra were collected for both the WT and R502W C3 samples as a function of temperature with a Jasco J-810 spectropolarimeter. The temperature was controlled using a Peltier thermoelectric system. Purified proteins (180 μL at a concentration of 15 μM) in buffer [20 mM sodium phosphate (pH 6.5) and 50 mM NaCl] were loaded into a 0.05 cm path-length quartz cuvette. Spectra, covering a wavelength range of 198−260 nm, were collected for the protein samples and buffer controls at 5 °C intervals between 20 and 70 °C. The samples were incubated at each temperature for 5 min before data were collected.

The collection of each set of data was repeated three times for the WT and R502W mutant. The buffer baseline spectrum was subtracted from each protein spectrum at each corresponding temperature to correct for the background signal. The sets of averaged spectra were deconvoluted into basis component spectra using the convex constraint algorithm in CCA+.[42] The sum of the fractions of the component spectra was normalized to 1 at each temperature. The change in the fraction of each basis spectrum, contributing to the total CD as a function of temperature, was used to monitor the transition between different folding stages. Protein unfolding, depicted by transitions between the component spectra, was plotted versus temperature. When the data points were fit with a Boltzmann sigmoidal curve[43−45] using GraphPad Prism version 5.00,[46] the midpoint unfolding temperatures were estimated.

Figure Preparation. Figures were prepared using PyMol.[39] The alignment figure was prepared using CLUSTALW[47] and ESPript.[48]

RESULTS

The WT and R502W C3 Domain in cMyBP-C Adopt an Ig-like Fold. Both the WT and R502W C3 domains yielded well-dispersed ^{15}N HSQC spectra (Figure S1 of the Supporting Information), confirming that they adopt independently folded structures when excised from the full-length protein. Using

dx.doi.org/10.1021/bi500784g | Biochemistry 2014, 53, 5332−5342

chemical shift-based dihedral angle restraints and an extensive set of NOE-derived distance restraints, the structural ensembles of the proteins were calculated with CYANA 3.0 (Figure 2a and Table 1). The resulting ensembles are well-defined with backbone atom rmsd values of 0.61 and 0.80 Å between residues 454−538 of the 10 lowest-energy structures in WT and R502W C3, respectively.

As expected from sequence analysis, the C3 domain adopts an Ig-like protein fold. This is a β-sandwich structure composed of two β-sheets with a Greek key topology (Figure S2 of the Supporting Information). The two sheets are formed by strands denoted as ABED and C′CFGG′A′ to maintain consistency with Ig fold nomenclature (Figure 2b,c). The β-sheets are antiparallel, except for the parallel arrangement of strand G′ with the short strand A′. Residues 519−522, which are part of the loop between strands E and F, fold into a short helix. This secondary structure description is consistent with that predicted by MICS[35] using chemical shifts.

The R502W Mutation Does Not Perturb the C3 Domain Structure. Globally, the structures of the WT and R502W C3 domains are highly similar, with a pairwise backbone rmsd of 1.37 ± 0.12 Å between their structural ensembles for residues 454−538 (Figure 3). Residue 502 is in the second position on strand D, and its backbone carbonyl and amide form hydrogen bonds with Ile513 (second to the last residue on strand E). Locally, substitution of Arg502 with tryptophan also did not perturb the structure of this sheet. In the WT protein ensemble, the side chain of Arg502 is not well-defined, adopting a range of conformations caused by the lack of any measurable distance restraints (Figure 3). Similarly, in the R502W mutant ensemble, the hydrophobic side chain of Trp502 also adopts a range of solvent-exposed orientations, again because of the lack of measurable restraints. Consistent with these minimal perturbations in the NMR-derived structural ensembles, the amide $^{1}H^{N}$ and ^{15}N chemical shift differences between the WT and R502W C3 domains are localized around position 502 (Figure S3 of the Supporting Information). Together, these data indicate that the R502W mutation does not alter the function of cMyBP-C through a large scale conformational change within the C3 domain itself.

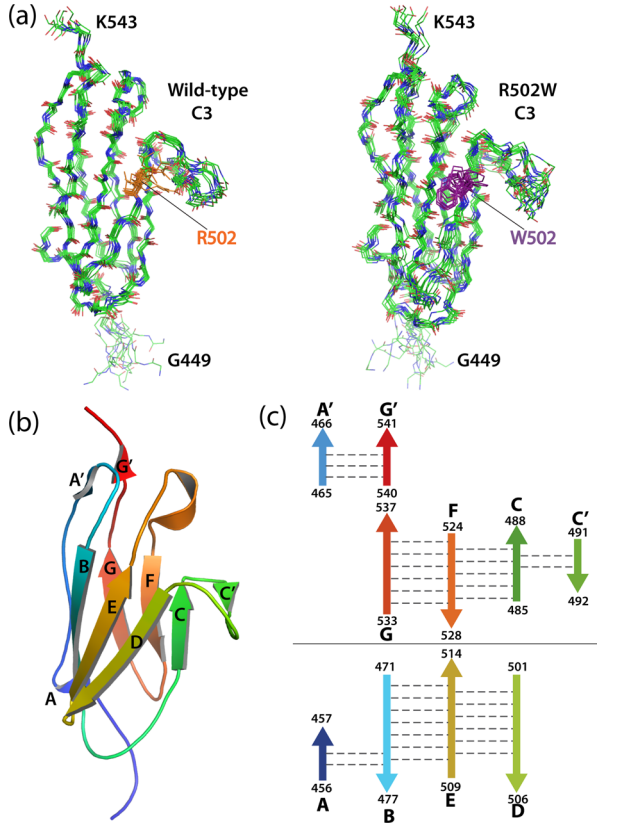

Figure 2. NMR-derived structural ensembles of the WT and R502W C3 domains. (a) The tertiary structural ensembles of the WT and R502W C3 domains are shown as main chain line diagrams (green for carbon, blue for nitrogen, and red for oxygen). The side chains of R502 (orange) and W502 (purple) are also highlighted. (b) The ribbon diagram presents the overall fold of the WT C3 domains. The β-strands are shown as arrows in rainbow colors from the N-terminus (blue) to the C-terminus (red). Two β-sheets are formed by strands ABED and C′CFGG′A′. (c) The hydrogen bonds between the β-strands are shown as gray dashed lines in a topology diagram, with the same coloring as in panel b. The two β-sheets are separated for the sake of clarity. The start and end residues of each β-strand are labeled.

The R502W Mutation Does Not Perturb the C3 Domain Dynamics. To characterize the nanosecond to picosecond dynamic properties of the WT and R502W C3 domains, amide ^{15}N T_1, T_2, and heteronuclear NOE relaxation data were collected for both proteins at 25 °C using a 500 MHz NMR spectrometer. From the T_1/T_2 ratios, global isotropic tumbling correlation times of 6.0 ± 0.03 and 5.7 ± 0.02 ns were determined for the WT and R502W mutant C3 domains, respectively. These correlation times are consistent with those expected for an 11 kDa protein[49] and thus confirm that both isolated C3 domains are monomeric.

The ^{15}N NOE values are very sensitive to the subnanosecond time scale motions of the $^{15}N-^{1}H^{N}$ bond vector and report on the local dynamics of the associated amino acid. In the mutant protein, the ^{15}N NOE value of the Trp502 indole $^{15}N^{\varepsilon 1}$ is 0.47 ± 0.01, whereas that of the buried Trp486 is 0.70 ± 0.01. The substantially lower ^{15}N NOE value indicates that the side chain of Trp502 in the R502W C3 domain is relatively mobile. This is expected from its solvent-exposed position and its multiple conformations in the structural ensemble caused by a lack of experimental distance restraints.

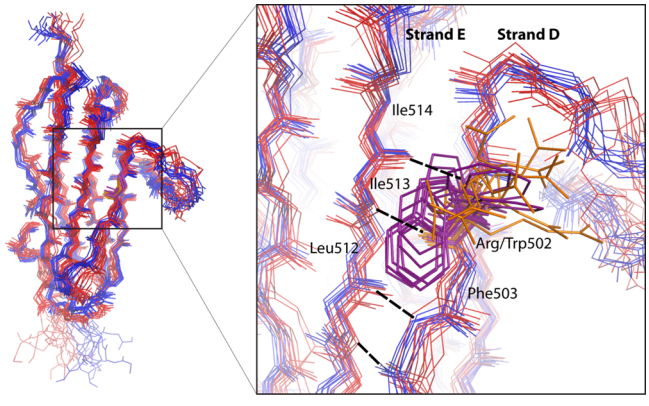

Figure 3. Structural superimposition of the WT and R502W C3 domains. Structural ensemble of the WT C3 domain (blue lines) overlaid on that of the R502W C3 domain (red lines). The region in the proximity of the R502W mutation is also shown in an expanded view, with the side chains of R502 (orange) and W502 (purple) shown as sticks. Hydrogen bonds between strands E and D are depicted as black dashed lines.

dx.doi.org/10.1021/bi500784g | Biochemistry 2014, 53, 5332−5342

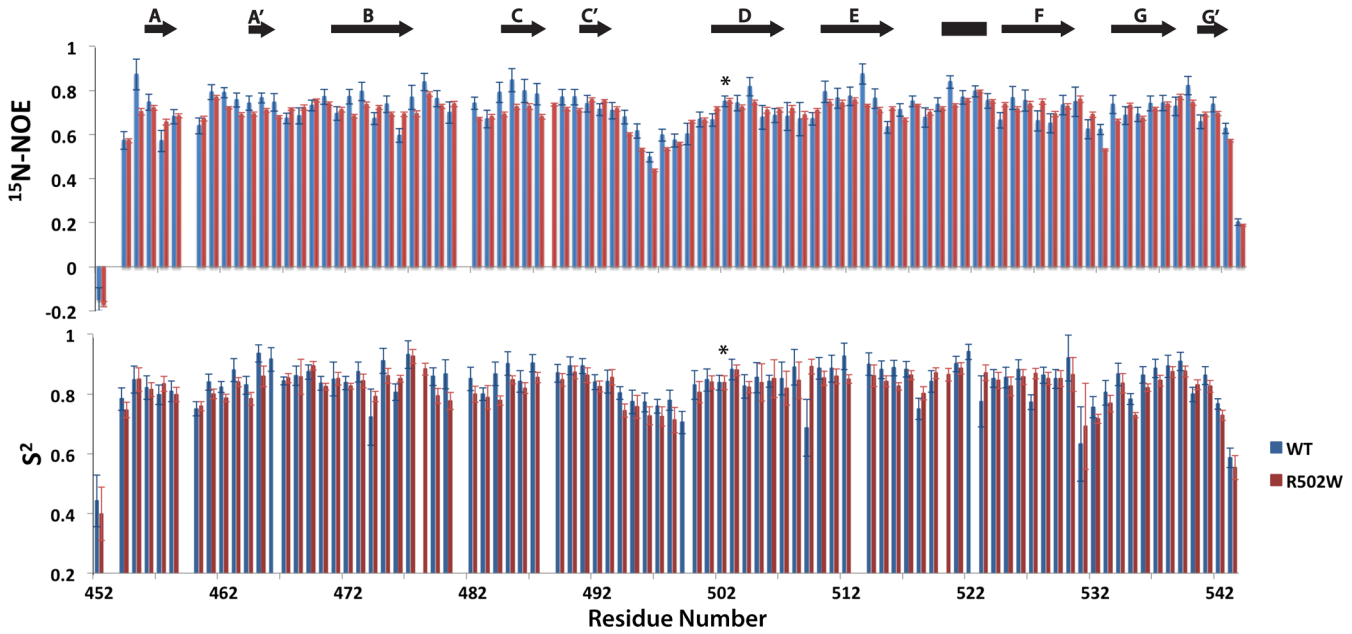

Figure 4. Backbone dynamics of the cMyBP-C C3 domains from amide ^{15}N relaxation analysis. Plots of ^{15}N NOE (top) and order parameter (S^2) values (bottom) vs residue number are shown for the WT (blue) and R502W (red) mutant C3 domain. Lower ^{15}N NOE and S^2 values, as seen for residues near the N- and C-termini and in the C′−D loop, are indicative of faster subnanosecond time scale backbone motions. Residue 502 is identified with an asterisk. The secondary structures identified in the 3D structures are mapped on top (arrows for β-strands and a rectangle for a helix).

The full sets of ^{15}N relaxation data for the main chain amides of both proteins were fit according to the anisotropic model-free formalism.[50] A comparison of these order parameters, as well as heteronuclear NOE values, indicates that both WT and R502W C3 domains exhibit very similar nanosecond to picosecond time scale motions (Figure 4). In each case, amides in β-strands are well-ordered, whereas those at the termini and in loop regions are somewhat more flexible. The most notable of the latter group are residues in the C′−D loop, which also show higher rmsd values in the structural ensembles calculated for each protein (Figure 2a).

As a sensitive probe of millisecond to microsecond time scale conformational exchange, the two proteins were investigated using ^{15}N amide relaxation dispersion measurements.[33] These studies revealed no conformational exchange for the WT or R502W C3 domain (data not shown). This is consistent with the model-free analysis in which the ^{15}N T_2 data for most amides were fit without the need for an additional T_2 exchange contribution. Collectively, these relaxation measurements demonstrate that substitution of Arg502 with tryptophan does not markedly change the dynamic properties of the C3 domains across a wide time scale range.

The R502W Mutation Does Not Affect the Thermal Stability of the C3 Domain. To investigate potential stability changes induced by the R502W mutation, the heat-induced denaturations of the WT and mutant were monitored using circular dichorism (CD) spectroscopy. Sets of spectra were collected over a temperature range from 20 to 70 °C (Figure 5a). With an increase in temperature, the minima of the spectra started at 217 nm (characteristic of β-sheets) and moved toward 200 nm (characteristic of random coils). This provides evidence that the C3 domain, mainly composed of β-sheets, was unfolding and losing its secondary structure as the temperature increased.

Using a convex constraint algorithm,[42] the collected sets of spectra were then deconvoluted into basis components. Two basis components (Figure 5b) were obtained, which suggests that the WT and R502W mutant both unfold in a predominantly global two-state transition. Upon obtaining the two basis components, we can interpret the spectrum collected at each temperature as the sum of fractions of each basis component. As the temperature changed from 20 to 70 °C, the fraction of one basis component decreased while the other increased.

The percentage of unfolding, depicted as the percentage of transition from one basis component spectra to the other as a function of temperature, is shown in Figure 5c. Data of both the WT and the R502W mutant fit well to Boltzmann sigmoidal curves. The unfolding profiles of the two proteins overlap closely (within the error range), with midpoint unfolding temperatures of 56.8 ± 2.0 °C for WT C3 and 55.4 ± 1.5 °C for mutant C3. This demonstrates that the R502W mutation did not have a significant impact on the overall thermal stability of the C3 domain.

The R502W Mutation Alters the Predicted C3 Domain Surface Charge. A comparison of the calculated Boltzmann−Poisson electrostatic features of the WT and R502W mutant C3 domains reveals a marked change in the surface charge induced by the R502W mutation (Figure 6). In WT C3, the side chains of Arg470, Lys485, Arg495, Arg502, Lys504, and Lys505 contribute to a large positively charged surface. This stands in contrast to the net negative charge on the remainder of the protein surface. Upon mutation of Arg502 to tryptophan, the size of the positively charged patch is reduced significantly. Such an electrostatic change could alter the interaction of the cMyBP-C C3 domain with a complementary charged partner protein.

dx.doi.org/10.1021/bi500784g | *Biochemistry* 2014, 53, 5332−5342

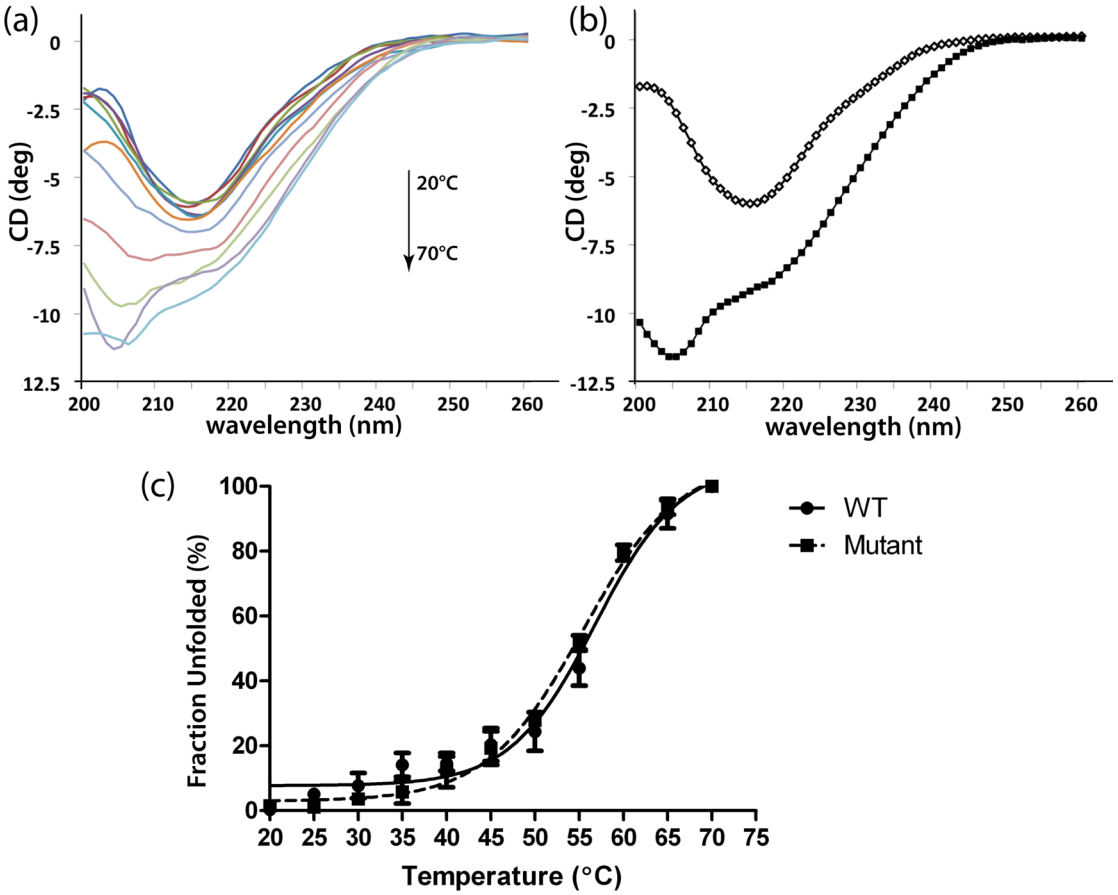

Figure 5. Temperature-induced unfolding of the C3 domain monitored by CD. (a) CD spectra of the WT C3 domain collected as a function of temperature. (b) Two deconvoluted basis component curves determined by the convex constraint algorithm for the WT C3 domain. Open squares correspond to the folded state and black squares correspond to unfolded state. The R502W C3 domain has spectra and basis component curves similar to those of the WT. (c) Data points of the fraction unfolded vs temperature follow Boltzmann-weighted sigmoidal curves, with R^2 values of 0.97 and 0.98 for the WT (round box) and R502W (square box) C3 domains, respectively. Each point on the plot (displayed with error bars) is an average of three experimental replicates.

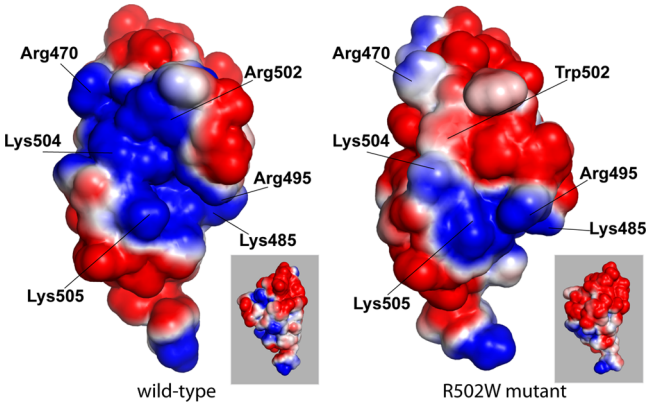

Figure 6. Electrostatic properties of the cMyBP-C C3 domain. Surface representations of the WT and R502W C3 domain, colored by electrostatic potential (negative, red; positive, blue) as calculated using default settings within the APBS[38] plug-in in PyMol.[67] The proteins are shown in the same orientation and rotated 180° along the long axis in the small insets. The residues that contribute to the positively charged patch are labeled.

DISCUSSION

The C3 Domain Belongs to the Immunoglobulin-like Family. Using NMR spectroscopy, we have shown that the isolated C3 domain of cMyBP-C adopts an Ig-like fold. This was not unexpected as, along with seven other domains within cMyBP-C, the C3 domain was predicted by sequence analysis to be Ig-like.[11] Indeed, this fold, which is composed of seven to nine antiparallel β-strands arranged in a Greek key β-sandwich,[51] has been reported in numerous proteins, including many non-immunoglobulins.[52] Strands B, C, E, and F are defined as the common core of Ig-like proteins[52] (Figure S2 of the Supporting Information). When compared with those of other Ig-like proteins, the lengths of the noncore strands and surrounding loops are highly variable, but these core strands are well-conserved.[53] Figure S4 of the Supporting Information shows a structural alignment of the C3 domain with six other proteins that are highly structurally similar. In this figure, the similarities of the core strands of the C3 domain to those of other Ig-like proteins can be clearly seen.

Like other Ig-like proteins, the C3 domain has three buried hydrophobic residues in its protein core, one from each of core strands B, C, and F.[54] In the cMyBP-C C3 domain, these are Phe473 on strand B, Trp486 on strand C, and Tyr525 on strand F. Also, in classical Ig domains, a disulfide bridge exists across the β-sandwich, formed between strands B and F.[51] However, this feature is not conserved in Ig-like proteins.[54] In the case of the cMyBP-C C3 domain, two cysteines are juxtaposed in strands B (Cys475) and F (Cys528). However,

dx.doi.org/10.1021/bi500784g | Biochemistry 2014, 53, 5332−5342

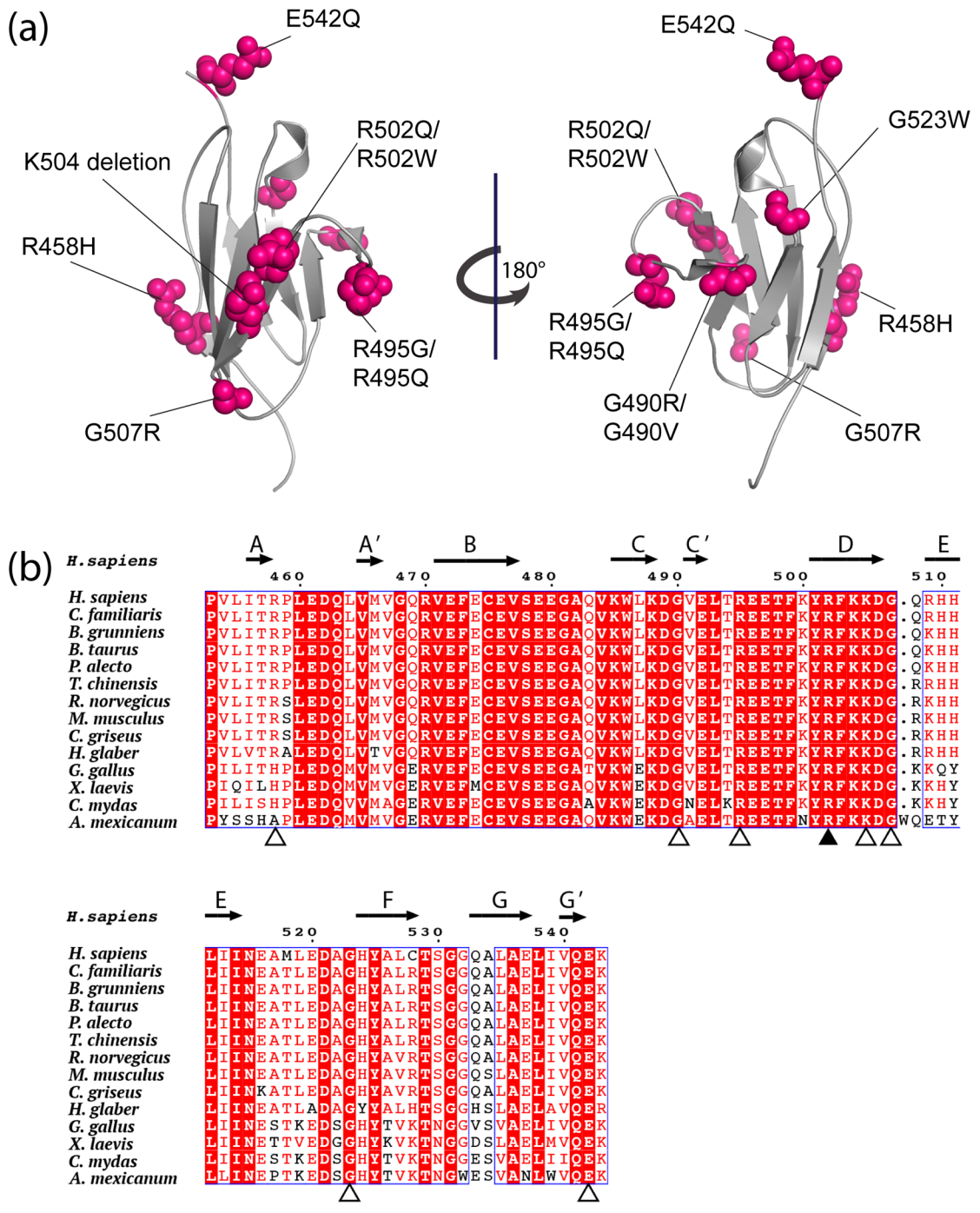

Figure 7. HCM-related mutations mapped onto the cMyBP-C C3 domain and cross-species alignment. (a) Positions of HCM-related mutations (R458H, G490R, G490V, R495G, R495Q, R502Q, R502W, Lys504 deletion, G507R, G523W, and E542Q) within the cMyBP-C C3 domain mapped onto the WT C3 structure (gray ribbon) as pink spheres. (b) Sequence alignment of C3 domains, with invariant residues in red boxes, similar residues in red text, and stretches of amino acids that are similar across the group of sequences in blue boxes. The NMR-derived secondary structure of the WT cMyBP-C C3 domain is shown above the alignment, which follows the *Homo sapiens* C3 sequence numbering. Arg502 is identified with a black arrowhead, and the remaining mutated residues in panel a are marked with white arrowheads. The protein sequences and the list of HCM-related mutations were acquired from the Swiss-Prot database:[68] *H. sapiens* (Q14896), *Canis familiariz* (Q2Q1P6), *Bos grunniens* (L8IEY5), *Bos taurus* (Q0VD56), *Pteropus alecto* (L5KZ62), *Tsuga chinensis* (L9JEW3), *Rattus norvegicus* (P56741), *Mus musculus* (Q3TF37), *Ceanothus griseus* (G3GYK6), *Heterocephalus glaber* (G5BPC6), *Gallus gallus* (E1C7T3), *Xenopus laevis* (Q90X86), *Chelonia mydas* (M7BYN8), and *Ambystoma mexicanum* (Q90233).

rather than pointing at each other, their side chains point in the same direction, preventing them from forming a disulfide bridge. The reduced states of Cys475 and Cys528 were confirmed from their highly diagnostic $^{13}C^{\beta}$ chemical shifts.[55]

The R502W Mutation May Disrupt Protein−Protein Interaction of the C3 Domain. The WT and R502W C3 domains are highly similar in terms of their structure (Figure 3), dynamics (Figure 4), and thermal stability (Figure 5). This strongly suggests that the functional consequences of the

dx.doi.org/10.1021/bi500784g | *Biochemistry* 2014, 53, 5332−5342

mutation do not arise via disruption of the structural integrity of the domain or through conformational rearrangements leading to allosteric effects. Rather, the mutation may directly alter the interactions of the C3 domain with cMyBP-C binding partners.

Cross-species alignment of the cMyBP-C C3 domain shows an overall high level of residue conservation, with Arg502 being invariant (Figure 7b). Furthermore, this arginine residue has been considered as a mutation "hot spot" because both R502Q and R502W mutations are related to HCM.[7] Our structural investigations suggest that Arg502 may play an important role in the proper functioning of the cMyBP-C C3 domain by contributing to an intermolecular interface.

Comparison of the electrostatic features of the WT and R502W mutant C3 domains shows that a large positively charged area on the surface of the protein is altered by the R502W mutation (Figure 6). Residues Arg470, Lys485, Arg495, Arg502, Lys504, and Lys505 form this positively charged patch on an otherwise negatively charged protein. The R502W mutation reduces this positively charged patch and thus could disrupt electrostatically guided protein interactions between the C3 domain and its protein binding partners. In addition, the mutation could eliminate direct interactions of the domain with such a partner via arginine-mediated salt bridges and hydrogen bonds.

cMyBP-C has been shown to interact with various proteins within the sarcomere. In its C-terminal region, domains C7−C10 bind to titin and light meromyosin (LMM).[13] In its N-terminal region (C0−C2 domains), the mybpc motif reaches out to interact with S2 of myosin in a phosphorylation-dependent manner,[17] while domains C0 and C1 and the (Pro-Ala)-rich motif may bind to myosin and/or actin.[18,21,22,56,57] The domain of interest in this study, the C3 domain, lies in the central region (C3−C6), which may be required for the flexibility of the N-terminal region, allowing it to interact with myosin S2 or actin. Because of its proximity to the N-terminal domains of cMyBP-C, the C3 domain may also be in contact with either of these potential partners, interacting with myosin or actin, at binding interfaces different from that of the N-terminal region. The C3 domain may also interact with myosin or actin during a different stage of the contraction cycle than that of the N-terminal region. The neighboring C2 domain is highly structurally similar to C3, and it has been shown to bind to myosin S2 in NMR monitored titration experiments and molecular modeling studies.[58] Similar to what we have proposed for the R502W mutation in the C3 domain, the modeling suggests that the key interactions are between polar amino acids and that HCM-related mutations (i.e., E301Q in C2 and R870H in S2) would disrupt these electrostatic interactions.

Actin is a negatively charged protein at physiological pH, and positively charged residues from a number of actin interacting partners have been implicated in actin-binding interfaces.[59−64] For example, one of the Ig-like domains in the C-terminal region of paladin has been shown to bind to actin in co-sedimentation assays.[65] We thus hypothesize that the positively charged patch on the C3 domain, to which Arg502 and five other residues contribute, may enhance an electrostatic interaction between cMyBP-C and actin. If so, the R502W mutation would disrupt this interaction, which could lead to the altered regulation of contractility in cardiac muscle and ultimately HCM. Our preliminary studies using isothermal titration calorimetry and surface plasmon resonance did not detect any binding between the isolated C3 domain and actin. However, it is possible that additional components of cMyBP-C are required for the postulated association with actin.

Other Hypertrophic Cardiomyopathy-Related Mutations in the C3 Domain. Eleven known mutations associated with HCM are in the C3 domain of cMyBP-C: R458H, G490R, G490V, R495G, R495Q, R502Q, R502W, Lys504 deletion, G507R, G523W, and E542Q. The positions of these mutations are mapped on the structure of the C3 domain and indicated within the cross-species sequence alignment (Figure 7). In each case, the side chains of all these residues are on the protein surface exposed to the solvent. As elaborated below, these 11 HCM-related mutations likely perturb electrostatically guided protein−protein interactions or, in the case of glycine substitutions, the proper folding of the C3 domain.

Several of these HCM-related mutations change conserved residues (Arg495, Arg502, and Lys504) that are positioned within the positively charged patch (Figure 6). This further highlights the importance of this surface in mediating protein−protein interactions and suggests a common mechanism for the disruption of function by these mutations. R458H and E542Q, which are not in the positively charged patch, may also contribute to the charge-mediated interactions of C3. Similar examples can be seen with mutations such as E258K and D228N in the C1 domain[66] and E301Q in the C2 domain,[58] all of which are HCM-related mutations and result in a change in the electrostatics of the protein surface.

The other observed HCM-linked mutations occur at glycine residues that are located within loop regions of the protein [e.g., Gly490 in the C−C′ loop, Gly507 in the D−E loop, and Gly523 in the E−F loop (Figure S5 of the Supporting Information)]. Gly490 is the third residue within a type II β-turn, in which the third residue is generally a glycine. Gly507 is part of a type I β-turn, sitting at the second residue position. Flanked by a short helix (residues 519−522) and strand F (residues 524−529), Gly523 is within a region with a high degree of curvature (defined as a "bend"), which means that the angle between the backbone of the residues before and after the bend has a directional change of >70°.[53] These glycines are presumably required for proper folding, and thus, the HCM-linked mutations at these sites may disrupt the structure of the C3 domain.

■ CONCLUSION

We have characterized in detail the WT and R502W C3 domains of human cardiac myosin binding protein C. The R502W mutation does not affect the conformation, dynamics, or thermal stability of the C3 domain. However, the R502W mutation reduces the size of a positively charged surface area on the protein. Electrostatic interactions occur between many sarcomeric proteins, and mutations that affect their surface charges have been shown to disrupt their interactions and possibly contribute to HCM. R502W appears to be one of the mutations that can impair the important electrostatic interactions of the C3 domain. Further research into the binding affinity and specificity of cMyBP-C with other sarcomeric proteins will provide more insight into these potential interactions and contribute to our understanding of the disease mechanisms of HCM.

■ ASSOCIATED CONTENT

Supporting Information

Figures S1−S5 provide additional details about the structures and their interpretation. This material is available free of charge via the Internet at http://pubs.acs.org.

■ AUTHOR INFORMATION

Corresponding Authors

*E-mail: mcintosh@chem.ubc.ca. Phone: (604) 822-3341. Fax: (604) 822-5227.

*E-mail: mpaetzel@sfu.ca. Phone: (778) 782-4320. Fax: (778) 782-5583.

Funding

This work was supported in part by the Canadian Institute of Health Research (M.P. and L.P.M.) and the National Science and Engineering Research Council of Canada (M.P. and L.P.M.). Instrument support was provided by the Canadian Institutes for Health Research, the Canada Foundation for Innovation, the British Columbia Knowledge Development Fund, the UBC Blusson Fund, and the Michael Smith Foundation for Health Research (MSFHR).

Notes

The authors declare no competing financial interest.

■ ABBREVIATIONS

HCM, hypertrophic cardiomyopathy; HSQC, heteronuclear single-quantum correlation; NMR, nuclear magnetic resonance; NOE, nuclear Overhauser enhancement; NOESY, nuclear Overhauser enhancement spectroscopy; cMyBP-C, cardiac myosin binding protein C; C3, C3 domain of cMyBP-C; WT, wild type.

■ REFERENCES

(1) Flashman, E., Redwood, C., Moolman-Smook, J., and Watkins, H. (2004) Cardiac myosin binding protein C: Its role in physiology and disease. *Circ. Res. 94*, 1279−1289.

(2) Harris, S. P., Bartley, C. R., Hacker, T. A., McDonald, K. S., Douglas, P. S., Greaser, M. L., Powers, P. A., and Moss, R. L. (2002) Hypertrophic cardiomyopathy in cardiac myosin binding protein-C knockout mice. *Circ. Res. 90*, 594−601.

(3) Seidman, J. G., and Seidman, C. (2001) The genetic basis for cardiomyopathy: From mutation identification to mechanistic paradigms. *Cell 104*, 557−567.

(4) Wang, L., Seidman, J. G., and Seidman, C. E. (2010) Narrative review: Harnessing molecular genetics for the diagnosis and management of hypertrophic cardiomyopathy. *Ann. Int. Med. 152*, 513.

(5) Watkins, H., Conner, D., Thierfelder, L., Jarcho, J. A., MacRae, C., McKenna, W. J., Maron, B. J., Seidman, J. G., and Seidman, C. E. (1995) Mutations in the cardiac myosin binding protein-C gene on chromosome 11 cause familial hypertrophic cardiomyopathy. *Nat. Genet. 11*, 434−437.

(6) Bonne, G., Carrier, L., Bercovici, J., Cruaud, C., Richard, P., Hainque, B., Gautel, M., Labeit, S., James, M., Beckmann, J., Weissenbach, J., Vosberg, H. P., Fiszman, M., Komajda, M., and Schwartz, K. (1995) Cardiac myosin binding protein-C gene splice acceptor site mutation is associated with familial hypertrophic cardiomyopathy. *Nat. Genet. 11*, 438−440.

(7) Richard, P., Charron, P., Carrier, L., Ledeuil, C., Cheav, T., Pichereau, C., Benaiche, A., Isnard, R., Dubourg, O., Burban, M., Gueffet, J., Millaire, A., Desnos, M., Schwartz, K., Hainque, B., and Komajda, M. (2003) Hypertrophic cardiomyopathy: Distribution of disease genes, spectrum of mutations, and implications for a molecular diagnosis strategy. *Circulation 107*, 2227−2232.

(8) Offer, G., Moos, C., and Starr, R. (1973) A new protein of the thick filaments of vertebrate skeletal myofibrils. Extractions, purification and characterization. *J. Mol. Biol. 74*, 653−676.

(9) Bennett, P., Craig, R., Starr, R., and Offer, G. (1986) The ultrastructural location of C-protein, X-protein and H-protein in rabbit muscle. *J. Muscle Res. Cell Motil. 7*, 550−567.

(10) Sjöström, M., and Squire, J. M. (1977) Fine structure of the A-band in cryo-sections. The structure of the A-band of human skeletal muscle fibres from ultra-thin cryo-sections negatively stained. *J. Mol. Biol. 109*, 49−68.

(11) Oakley, C. E., Hambly, B. D., Curmi, P. M. G., and Brown, L. J. (2004) Myosin binding protein C: Structural abnormalities in familial hypertrophic cardiomyopathy. *Cell Res. 14*, 95−110.

(12) Gautel, M., Zuffardi, O., Freiburg, A., and Labeit, S. (1995) Phosphorylation switches specific for the cardiac isoform of myosin binding protein-C: A modulator of cardiac contraction? *EMBO J. 14*, 1952−1960.

(13) Gilbert, R., Kelly, M. G., Mikawa, T., and Fischman, D. A. (1996) The carboxyl terminus of myosin binding protein C (MyBP-C, C-protein) specifies incorporation into the A-band of striated muscle. *J. Cell Sci. 109* (Part 1), 101−111.

(14) Okagaki, T., Weber, F. E., Fischman, D. A., Vaughan, K. T., Mikawa, T., and Reinach, F. C. (1993) The major myosin-binding domain of skeletal muscle MyBP-C (C protein) resides in the COOH-terminal, immunoglobulin C2 motif. *J. Cell Biol. 123*, 619−626.

(15) Flashman, E., Watkins, H., and Redwood, C. (2007) Localization of the binding site of the C-terminal domain of cardiac myosin-binding protein-C on the myosin rod. *Biochem. J. 401*, 97−102.

(16) Kunst, G., Kress, K. R., Gruen, M., Uttenweiler, D., Gautel, M., and Fink, R. H. (2000) Myosin binding protein C, a phosphorylation-dependent force regulator in muscle that controls the attachment of myosin heads by its interaction with myosin S2. *Circ. Res. 86*, 51−58.

(17) Gruen, M., Prinz, H., and Gautel, M. (1999) cAPK-phosphorylation controls the interaction of the regulatory domain of cardiac myosin binding protein C with myosin-S2 in an on-off fashion. *FEBS Lett. 453*, 254−259.

(18) Squire, J. M., Luther, P. K., and Knupp, C. (2003) Structural evidence for the interaction of C-protein (MyBP-C) with actin and sequence identification of a possible actin-binding domain. *J. Mol. Biol. 331*, 713−724.

(19) Witayavanitkul, N., Ait Mou, Y., Kuster, D. W. D., Khairallah, R. J., Sarkey, J., Govindan, S., Chen, X., Ge, Y., Rajan, S., Wieczorek, D. F., Irving, T., Westfall, M. V., de Tombe, P. P., and Sadayappan, S. (2014) Myocardial infarction-induced N-terminal fragment of cardiac myosin-binding protein C (cMyBP-C) impairs myofilament function in human myocardium. *J. Biol. Chem. 289*, 8818−8827.

(20) Howarth, J. W., Ramisetti, S., Nolan, K., Sadayappan, S., and Rosevear, P. R. (2012) Structural insight into unique cardiac myosin-binding protein-C motif: A partially folded domain. *J. Biol. Chem. 287*, 8254−8262.

(21) Shaffer, J. F., and Harris, S. P. (2009) Species-specific differences in the Pro-Ala rich region of cardiac myosin binding protein-C. *J. Muscle Res. Cell Motil. 30*, 303−306.

(22) Mun, J. Y., Gulick, J., Robbins, J., Woodhead, J., Lehman, W., and Craig, R. (2011) Electron microscopy and 3D reconstruction of F-actin decorated with cardiac myosin-binding protein C (cMyBP-C). *J. Mol. Biol. 410*, 214−225.

(23) Wilkins, M. R., Gasteiger, E., Bairoch, A., Sanchez, J. C., Williams, K. L., Appel, R. D., and Hochstrasser, D. F. (1999) Protein identification and analysis tools in the ExPASy server. *Methods Mol. Biol. 112*, 531−552.

(24) Delaglio, F., Grzesiek, S., Vuister, G. W., Zhu, G., Pfeifer, J., and Bax, A. (1995) NMRPipe: A multidimensional spectral processing system based on UNIX pipes. *J. Biomol. NMR 6*, 277−293.

(25) Goddard, T. D., and Kneller, D. G. (1999) *SPARKY 3*, University of California, San Francisco.

(26) Sattler, M., Schleucher, J., and Griesinger, C. (1999) Heteronuclear multidimensional NMR experiments for the structure

determination of proteins in solution employing pulsed field gradients. *Prog. Nucl. Magn. Reson. Spectrosc. 34*, 93−158.
(27) Yamazaki, T., Forman-Kay, J. D., and Kay, L. E. (1993) Two dimensional NMR experiment for correlating $^{13}C\beta$ and $^{1}H\delta/\varepsilon$ chemical shifts of aromatic residues in ^{13}C labeled proteins via scalar couplings. *J. Am. Chem. Soc. 115*, 11054−11055.
(28) Shen, Y., Delaglio, F., Cornilescu, G., and Bax, A. (2009) TALOS+: A hybrid method for predicting protein backbone torsion angles from NMR chemical shifts. *J. Biomol. NMR 44*, 213−223.
(29) Zwahlen, C., Gardner, K. H., Sarma, S. P., Horita, D. A., Byrd, R. A., and Kay, L. E. (1998) An NMR experiment for measuring methyl−methyl NOEs in ^{13}C-labeled proteins with high resolution. *J. Am. Chem. Soc. 120* (30), 7617−7625.
(30) Güntert, P. (2004) Automated NMR structure calculation with CYANA. *Methods Mol. Biol. 278*, 353−378.
(31) Brunger, A. T., Adams, P. D., Clore, G. M., DeLano, W. L., Gros, P., Grosse-Kunstleve, R. W., Jiang, J. S., Kuszewski, J., Nilges, M., Pannu, N. S., Read, R. J., Rice, L. M., Simonson, T., and Warren, G. L. (1998) Crystallography & NMR system: A new software suite for macromolecular structure determination. *Acta Crystallogr. D54*, 905−921.
(32) Farrow, N. A., Muhandiram, R., Singer, A. U., Pascal, S. M., Kay, C. M., Gish, G., Shoelson, S. E., Pawson, T., Forman-Kay, J., and Kay, L. E. (1994) Backbone dynamics of a free and phosphopeptide-complexed src homology 2 domain studied by ^{15}N NMR relaxation. *Biochemistry 33*, 5984−6003.
(33) Dosset, P., Hus, J. C., Blackledge, M., and Marion, D. (2000) Efficient analysis of macromolecular rotational diffusion from heteronuclear relaxation data. *J. Biomol. NMR 16*, 23−28.
(34) Tollinger, M., Skrynnikov, N. R., Mulder, F. A., Forman-Kay, J., and Kay, L. E. (2001) Slow dynamics in folded and unfolded states of an SH3 domain. *J. Am. Chem. Soc. 123*, 11341−11352.
(35) Shen, Y., and Bax, A. (2012) Identification of helix capping and β-turn motifs from NMR chemical shifts. *J. Biomol. NMR 52*, 211−232.
(36) Holm, L., and Rosenström, P. (2010) Dali server: Conservation mapping in 3D. *Nucleic Acids Res. 38*, W545−W549.
(37) Ye, Y., and Godzik, A. (2003) Flexible structure alignment by chaining aligned fragment pairs allowing twists. *Bioinformatics 19* (Suppl. 2), ii246−ii255.
(38) Baker, N. A., Sept, D., Joseph, S., Holst, M. J., and McCammon, J. A. (2001) Electrostatics of nanosystems: Application to microtubules and the ribosome. *Proc. Natl. Acad. Sci. U.S.A. 98*, 10037−10041.
(39) DeLano, W. L. (2004) Use of PYMOL as a communications tool for molecular science. *Abstracts of Papers of the American Chemical Society*, Vol. *228*, pp U313−U314, American Chemical Society, Washington, DC.
(40) Wang, J., Cieplak, P., and Kollman, P. A. (2000) How well does a restrained electrostatic potential (RESP) model perform in calculating conformational energies of organic and biological molecules? *J. Comput. Chem. 21* (12), 1049−1074.
(41) Dolinsky, T. J., Nielsen, J. E., McCammon, J. A., and Baker, N. A. (2004) PDB2PQR: An automated pipeline for the setup of Poisson-Boltzmann electrostatics calculations. *Nucleic Acids Res. 32*, W665−W667.
(42) Perczel, A., Hollósi, M., Tusnády, G., and Fasman, G. D. (1991) Convex constraint analysis: A natural deconvolution of circular dichroism curves of proteins. *Protein Eng. 4*, 669−679.
(43) Liu, W., Hanson, M. A., Stevens, R. C., and Cherezov, V. (2010) LCP-tm: An assay to measure and understand stability of membrane proteins in a membrane environment. *Biophys. J. 98*, 1539−1548.
(44) Orwig, S. D., and Lieberman, R. L. (2011) Biophysical characterization of the olfactomedin domain of myocilin, an extracellular matrix protein implicated in inherited forms of glaucoma. *PLoS One 6*, e16347.
(45) Niesen, F. H., Berglund, H., and Vedadi, M. (2007) The use of differential scanning fluorimetry to detect ligand interactions that promote protein stability. *Nat. Protoc. 2*, 2212−2221.
(46) *GraphPad Prism Version 5.00 for Windows* (2007) GraphPad Software, San Diego.
(47) Larkin, M. A., Blackshields, G., Brown, N. P., Chenna, R., McGettigan, P. A., McWilliam, H., Valentin, F., Wallace, I. M., Wilm, A., Lopez, R., Thompson, J. D., Gibson, T. J., and Higgins, D. G. (2007) Clustal W and clustal X version 2.0. *Bioinformatics 23*, 2947−2948.
(48) Gouet, P., Courcelle, E., Stuart, D. I., and Métoz, F. (1999) ESPript: Analysis of multiple sequence alignments in PostScript. *Bioinformatics 15*, 305−308.
(49) Daragan, V. A., and Mayo, K. H. (1997) Motional model analyses of protein and peptide dynamics using ^{13}C and ^{15}N NMR relaxation. *Prog. Nucl. Magn. Reson. Spectrosc. 31* (1), 63−105.
(50) Lipari, G., and Szabo, A. (1982) Model-free approach to the interpretation of nuclear magnetic resonance relaxation in macromolecules. 1. Theory and range of validity. *J. Am. Chem. Soc. 104*, 4546−4559.
(51) Lesk, A. M., and Chothia, C. (1982) Evolution of proteins formed by β-sheets. II. The core of the immunoglobulin domains. *J. Mol. Biol. 160*, 325−342.
(52) Bork, P., Holm, L., and Sander, C. (1994) The immunoglobulin fold. Structural classification, sequence patterns and common core. *J. Mol. Biol. 242*, 309−320.
(53) Kabsch, W., and Sander, C. (1983) Dictionary of protein secondary structure: Pattern recognition of hydrogen-bonded and geometrical features. *Biopolymers 22*, 2577−2637.
(54) Halaby, D. M., Poupon, A., and Mornon, J. (1999) The immunoglobulin fold family: Sequence analysis and 3D structure comparisons. *Protein Eng. 12*, 563−571.
(55) Sharma, D., and Rajarathnam, K. (2000) ^{13}C NMR chemical shifts can predict disulfide bond formation. *J. Biomol. NMR 18* (2), 165−171.
(56) Witt, C. C., Gerull, B., Davies, M. J., Centner, T., Linke, W. A., and Thierfelder, L. (2001) Hypercontractile properties of cardiac muscle fibers in a knock-in mouse model of cardiac myosin-binding protein-C. *J. Biol. Chem. 276*, 5353−5359.
(57) Kulikovskaya, I., McClellan, G., Flavigny, J., Carrier, L., and Winegrad, S. (2003) Effect of MyBP-C binding to actin on contractility in heart muscle. *J. Gen. Physiol. 122*, 761−774.
(58) Ababou, A., Gautel, M., and Pfuhl, M. (2007) Dissecting the N-terminal myosin binding site of human cardiac myosin-binding protein C. Structure and myosin binding of domain C2. *J. Biol. Chem. 282*, 9204−9215.
(59) Amann, K. J., Renley, B. A., and Ervasti, J. M. (1998) A cluster of basic repeats in the dystrophin rod domain binds F-actin through an electrostatic interaction. *J. Biol. Chem. 273*, 28419−28423.
(60) de Arruda, M. V., Bazari, H., Wallek, M., and Matsudaira, P. (1992) An actin footprint on villin. Single site substitutions in a cluster of basic residues inhibit the actin severing but not capping activity of villin. *J. Biol. Chem. 267*, 13079−13085.
(61) Hüttelmaier, S., Harbeck, B., Steffens, O., Messerschmidt, T., Illenberger, S., and Jockusch, B. M. (1999) Characterization of the actin binding properties of the vasodilator-stimulated phosphoprotein VASP. *FEBS Lett. 451*, 68−74.
(62) Janssen, M. E. W., Kim, E., Liu, H., Fujimoto, L. M., Bobkov, A., Volkmann, N., and Hanein, D. (2006) Three-dimensional structure of vinculin bound to actin filaments. *Mol. Cell 21*, 271−281.
(63) Lee, H., Bellin, R. M., Walker, D. L., Patel, B., Powers, P., Liu, H., Garcia-Alvarez, B., de Pereda, J. M., Liddington, R. C., Volkmann, N., Hanein, D., Critchley, D. R., and Robson, R. M. (2004) Characterization of an actin-binding site within the talin FERM domain. *J. Mol. Biol. 343*, 771−784.
(64) Yarmola, E. G., Edison, A. S., Lenox, R. H., and Bubb, M. R. (2001) Actin filament cross-linking by MARCKS: Characterization of two actin-binding sites within the phosphorylation site domain. *J. Biol. Chem. 276*, 22351−22358.
(65) Dixon, R. D. S., Arneman, D. K., Rachlin, A. S., Sundaresan, N. R., Costello, M. J., Campbell, S. L., and Otey, C. A. (2008) Palladin is

an actin cross-linking protein that uses immunoglobulin-like domains to bind filamentous actin. *J. Biol. Chem. 283*, 6222−6231.
(66) Govada, L., Carpenter, L., da Fonseca, P. C., Helliwell, J. R., Rizkallah, P., Flashman, E., Chayen, N. E., Redwood, C., and Squire, J. M. (2008) Crystal structure of the C1 domain of cardiac myosin binding protein-C: Implications for hypertrophic cardiomyopathy. *J. Mol. Biol. 378*, 387−397.
(67) DeLano, W. L. (2002) *PyMOL molecular graphics system*, DeLano Scientific, San Carlos, CA.
(68) The UniProt Consortium (2014) Activities at the universal protein resource (UniProt). *Nucleic Acids Res. 42*, D191−D198.